Video Article

Analysis of the Gap Junction-dependent Transfer of miRNA with 3D-FRAP Microscopy

Heiko Lemcke[1,2,3], Natalia Voronina[1,2,3], Gustav Steinhoff[1,2,3], Robert David[1,2,3]

[1]Reference and Translation Center for Cardiac Stem Cell Therapy (RTC)

[2]Department of Cardiac Surgery, University of Rostock

[3]Department of Life, Light and Matter of the Interdisciplinary Faculty, University of Rostock

Correspondence to: Heiko Lemcke at heiko.lemcke@uni-rostock.de, Robert David at davidrob@med.uni-rostock.de

URL: https://www.jove.com/video/55870
DOI: doi:10.3791/55870

Keywords: Cellular Biology, Issue 124, gap junctions, miRNA transfer, intercellular communication, fluorescence recovery after photobleaching, FRAP, photobleaching

Date Published: 6/19/2017

Citation: Lemcke, H., Voronina, N., Steinhoff, G., David, R. Analysis of the Gap Junction-dependent Transfer of miRNA with 3D-FRAP Microscopy. *J. Vis. Exp.* (124), e55870, doi:10.3791/55870 (2017).

Abstract

Small antisense RNAs, like miRNA and siRNA, play an important role in cellular physiology and pathology and, moreover, can be used as therapeutic agents in the treatment of several diseases. The development of new, innovative strategies for miRNA/siRNA therapy is based on an extensive knowledge of the underlying mechanisms. Recent data suggest that small RNAs are exchanged between cells in a gap junction-dependent manner, thereby inducing gene regulatory effects in the recipient cell. Molecular biological techniques and flow cytometric analysis are commonly used to study the intercellular exchange of miRNA. However, these methods do not provide high temporal resolution, which is necessary when studying the gap junctional flux of molecules. Therefore, to investigate the impact of miRNA/siRNA as intercellular signaling molecules, novel tools are needed that will allow for the analysis of these small RNAs at the cellular level. The present protocol describes the application of three-dimensional fluorescence recovery after photobleaching (3D-FRAP) microscopy to elucidating the gap junction-dependent exchange of miRNA molecules between cardiac cells. Importantly, this straightforward and non-invasive live-cell imaging approach allows for the visualization and quantification of the gap junctional shuttling of fluorescently labeled small RNAs in real time, with high spatio-temporal resolution. The data obtained by 3D-FRAP confirm a novel pathway of intercellular gene regulation, where small RNAs act as signaling molecules within the intercellular network.

Video Link

The video component of this article can be found at https://www.jove.com/video/55870/

Introduction

Small noncoding RNAs are important players in cellular gene regulation. These molecules are composed of 20-25 nucleotides that bind to a specific target mRNA, leading to the blockage of translation or to mRNA degradation[1,2]. The gene regulatory process undertaken by small RNAs, such as miRNA and siRNA, is a highly conserved mechanism that has been found in many different species[3]. In particular, miRNA molecules are of crucial importance to a variety of physiological processes, including proliferation, differentiation, and regeneration[4,5]. In addition, the dysregulation of miRNA expression is attributed to many pathological disorders. Correspondingly, miRNAs have been demonstrated to be suitable as biomarkers for diagnosis and as therapeutic agents for gene therapy[6,7].

Gap junctions (GJs) are specialized protein structures in the plasma membrane of two adjacent cells that allow the diffusional exchange of molecules with a molecular weight of up to 1 kD. They have been shown to be important to tissue development, differentiation, cell death, and pathological disorders such as cancer or cardiovascular disease[8,9,10]. Several molecules have been described as being capable of crossing GJ channels, including ions, metabolites, and nucleotides. Interestingly, GJs were also found to provide a pathway for the intercellular movement of small RNAs[11,12]. Thus, miRNAs can act not only within the cell in which they are produced, but also within recipient cells. This highlights the role of miRNAs in the intercellular signal transduction system. At the same time, the data demonstrate that gap junctional intercellular communication is closely linked to miRNA function. Because of the significant impact of miRNA and GJs on tissue homeostasis, pathology, and diagnosis, a comprehensive understanding of the function of GJs and the related intercellular dynamics of miRNA will help to clarify the mechanisms of miRNA-based diseases and to develop new strategies for miRNA therapies.

Depending on the extent of gap junctional coupling, the transfer of miRNA molecules between cells can be a very rapid process. Therefore, a methodology that allows the visualization and quantification of the fast intercellular movement of these regulatory signaling molecules is required. Commonly, flow cytometry and molecular biological techniques have been applied to demonstrate the shuttling of small RNAs[11,12,13,14]. However, as opposed to FRAP microscopy, these approaches lack high temporal resolution, which is mandatory when analyzing the exchange of miRNA via GJs. Moreover, FRAP microscopy is less invasive and therefore represents a powerful and novel live-cell imaging technique to evaluate the GJ-dependent exchange of molecules in several cell types[15,16,17].

Here, we present a detailed protocol describing the application of 3D-FRAP to assess miRNA shuttling between cardiomyocytes. For this purpose, cardiomyocytes were transfected with fluorescently labeled miRNA. A cell marked with this miRNA was photobleached, and the gap junctional miRNA re-influx from adjacent cells was recorded in a time-dependent manner. The high temporal resolution of FRAP experiments offers the possibility to perform kinetic studies for the precise evaluation of the intercellular transfer of miRNA and siRNA between living cells. Moreover, as small RNAs can be exchanged via different mechanisms with highly different kinetics, FRAP microscopy can help to clarify the extent to which GJs are involved in the respective shuttling processes[18]. In addition, 3D-FRAP can be used to investigate physiological and pathological alterations in GJ permeability and its impact on small RNA transfer[15,19].

Protocol

All steps in this protocol involving neonatal mice were performed per the ethical guidelines for animal care of the Rostock University Medical Centre.

1. Preparation of Cell Culture Dishes and the Medium for Cardiomyocyte Culture

1. Coat a cell culture plate with 0.1% gelatin in PBS and incubate at 37 °C for 4 h or at 4 °C overnight. Remove the gelatin and allow it to dry under sterile laminar air flow.
2. Prepare cell culture medium composed of 50 mL of DMEM supplemented with 10% fetal bovine serum (FBS) and 1% penicillin/streptomycin (P/S). Pre-warm it to 37 °C.

2. Isolation of Neonatal Cardiomyocytes

1. Sacrifice neonatal mice (1-2 days old) by decapitation with sterile scissors and open the chest along the sternum. Remove the heart using forceps while slightly pressing the thorax together and transfer the heart into a 24-well plate containing ice-cold HBSS (without Ca^{2+} and Mg^{2+}).
2. Remove non-cardiac tissue and larger vessels using sterile forceps. Transfer cleaned hearts into a 1.5 mL tube containing ice-cold HBSS. Use a maximum of 5 hearts per tube for enzymatic digestion.
3. Mince the hearts with small scissors into <0.5 to 1 mm^3 pieces.
4. Wash the minced hearts with HBSS two times by aspiration/addition of HBSS using a 1-mL microliter pipette. Remove the HBSS completely before adding the enzymes.
5. For the enzymatic digestion of neonatal hearts, use a commercially available kit and follow the manufacturer's protocol (see the **Table of Materials**). Shake the tube containing the minced hearts every 5 min while incubating with enzymes at 37 °C for 35 min.
6. Seed suspended cells on non-coated cell culture dishes containing cell culture medium for 1.5-2 h to allow the adherence of the non-cardiomyocyte fraction. Repeat this step if a high purity of cardiomyocytes is needed. If desired, further culture the non-cardiomyocyte fraction.
   NOTE: For a cell suspension of 15 hearts, the pre-plating step can be performed on 75 cm^2 cell culture flasks. Usually, ~5 x 10^5 cells are obtained from one neonatal heart.
7. Collect the supernatant in a 15 mL conical tube and centrifuge for 10 min at 300 x g. Resuspend the cells in 1 mL of cell culture medium.
8. Count the cells with a Neubauer chamber hemocytometer, or use an equivalent method.
9. Plate isolated cardiomyocytes on 6-well plates with a density of 3 x 10^5 cells/cm^2. Incubate the cells overnight at 37 °C and 5% CO_2.
   NOTE: Optionally, cells can also be transfected at this point. However, increased viability was observed when the cells were cultured for one day before being subjected to electroporation.

3. Transfection with Fluorescently Labeled miRNA

1. Pre-warm cell culture medium (see step 1.2) to 37 °C in a water bath or an equivalent device.
2. Prepare a 20 µM stock solution of fluorescent miRNA in RNase-free sterile water.
3. Prepare electroporation buffer containing 90 mM Na_2HPO_4, 90 mM NaH_2PO_4, 5 mM KCl, 10 mM $MgCl_2$, and 10 mM sodium succinate and adjust the pH to 7.2; electroporation buffer can be stored at -20 °C for several months.
4. Detach the cells from the culture dish using 0.05% trypsin for 5 min. Inactivate the trypsin by adding cell culture medium.
5. Count the cells with a Neubauer chamber hemocytometer, or use an equivalent method. Centrifuge the cells at 300 x g for 10 min.
6. Resuspend the cells in electroporation buffer to obtain a concentration of 4 x 10^5 cells per 100 µL.
7. **Mix 100 µL of cell suspension with fluorescent miRNA (final concentration: 0.25 µM) in a tube and load the mixture into an electroporation cuvette.**
   1. Empirically determine the appropriate amount of miRNA, depending upon cell type.
8. Perform electroporation using an electroporation device (see the **Table of Materials**), using the "G-009" program.
9. Add 500 µL of pre-warmed cell culture medium and transfer the whole cell suspension (4 x 10^5 cells) into a well of a 4-well glass-bottom chamber slide. Culture the cells for 1 day at 37 °C in a 5% CO_2 atmosphere.
   NOTE: For FRAP analysis, a cell density of ~80% is optimal. The transfection of labeled miRNA should exclusively be performed using electroporation. Since the homogenous distribution of labeled miRNA molecules is beneficial for FRAP measurement, reagent-based transfection is not recommended.

4. Applying 3D-FRAP Microscopy (Day 3)

1. Warm up the microscope incubator to 37 °C and switch on the confocal microscope system at least 2 h before FRAP measurement to establish a thermal equilibrium and to decrease the possibility of drift. If possible, maintain a 5% CO_2 atmosphere.

2. Insert the chamber slide into the stage sample holder.
3. Find a cluster of transfected cardiomyocytes using a 1.4 N.A. oil objective (400X magnification) and 561-nm laser excitation light at low laser power, with a detection range of 570-680 nm.
   NOTE: The definition of FRAP settings, the image acquisition, and the analysis were done using microscope-specific software (see the **Table of Materials**).
4. **Activate the "z-Stack," "Time Series," "Bleaching," and "Regions" buttons in the "Setup Manager."**
5. **Define the FRAP parameters.**
   1. Define the image acquisition settings in the "Acquisition Mode" menu by setting the "frame size" to 512 x 512, the "line step" to 1, and the "scan time" to <1 s.
   2. In the "Channels" menu, adjust the laser power, offset, and gain settings to obtain maximal fluorescence from minimal laser excitation (*e.g.,* laser power: 1-5%); adjust to avoid intensity saturation. Set the "pinhole size" to 2 µm.
   3. Next, in the "Regions" menu, select the "ROI drawing tool" and use the cursor to mark the target cell, the reference cell, and the background area. If required, select several target cells for photobleaching.
   4. Adjust the photobleaching settings in the "Bleaching" menu (*e.g.,* iterations: 9-14, laser power for photobleaching: 100%, interval of image acquisition: 60 s, cycles: 15). Define the start of bleaching after 3 initial scans.
   5. In the "z-Stack" menu, define the limits for z-stack acquisition, depending on the thickness of the cells. Adjust the "number of z-layers" to 12 - 15.
   6. Start the FRAP experiment and record the fluorescence recovery.
      NOTE: Since the settings of a FRAP experiment depend upon the cell type, the fluorescent dye, and the microscope system, it is best to perform pilot experiments to determine the optimal parameters for FRAP. Bleaching should be sufficient to reduce the initial fluorescence intensity by at least 50%. Typically, fluorescence recovery should be recorded every 30-60 s until the plateau phase is reached.

5. Data Analysis

1. **Create maximum projections of the acquired z-stacks and obtain fluorescence intensity values of the bleached target cells, the reference cell, and the background. Using microscope-specific software, click "Processing" → "Maximum intensity projection" → select file → "Apply."**
   1. Alternatively, use an equivalent image analyzing tool (*e.g.,* ImageJ).

2. **Copy the fluorescence intensity data at all time points from the target cell, the background, and the reference cell into a spreadsheet.**
   1. Subtract the background intensity and the intensity of the reference cell from the intensity values of the target cell to correct for photobleaching caused during the acquisition process. Perform background and reference cell corrections for each time point.
   2. Normalize the corrected FRAP data to the initial fluorescence intensity before bleaching by dividing each value by the initial fluorescence.
   3. To obtain FRAP curves, set the baseline to the fluorescence intensity immediately after the bleach by subtracting from the intensity values of each time point.

Representative Results

Here, we present 3D-FRAP microscopy as a non-invasive technique to study the gap junctional shuttling of fluorescent miRNA within neonatal cardiomyocytes. The isolated cardiomyocytes revealed the typical striated α-actinin pattern and contained large plaques of Cx43 along the cell-cell borders (**Figure 1A**, white arrowheads), which allowed for the high intercellular flux of molecules. The purity of isolated cardiomyocytes was assessed by the microscopic quantification of α-actinin-positive cells. Although some non-cardiomyocytes (α-actinin-negative cells) were present in the culture, neonatal cardiomyocytes represented the major cell type after isolation (79.62 ± 3.68%; **Figure 1B**).

To investigate the gap junctional exchange of miRNA, cells were transfected with fluorescently labeled miRNA. Electroporation is the method of choice to deliver miRNA molecules to cells, as it ensures a high transfection efficiency and the homogenous distribution of transfected compounds, which is mandatory for FRAP analysis. In our experimental setup, we achieved a transfection efficiency of ~ 45%, as determined by flow cytometry (**Figure 2A**). The preparation of cardiomyocytes for FRAP includes detachment from the culture plate, electroporation, and re-attachment onto chamber slides. A flow cytometric live/dead assay revealed that the majority of cells demonstrated high viability, which is important when analyzing gap junctional communication (**Figure 2B**). Moreover, cell density is a crucial parameter that affects FRAP results. For optimal FRAP measurements, cells should be seeded with a density of ~80% to allow for the formation of cell clusters and the establishment of functional gap junctions between cells (**Figure 2C**).

For FRAP analysis, target cells are selected within a cell cluster and are photobleached with 100% laser power, leading to reduced miRNA fluorescence in the selected cells (**Figure 3A**, bleach). Subsequently, fluorescence recovery is recorded to visualize the transfer of miRNA from adjacent cells into the bleached area. Since the plateau phase of the fluorescence recovery was reached after 13 min, this time span was used for image acquisition in the FRAP experiments. Quantitative analysis and normalization of the acquired data showed an average recovery of 20%. The data also demonstrated that FRAP microscopy allows for the rapid recording of miRNA shuttling with high temporal resolution. Depending on the dye properties, acquisition parameters can be changed to further increase temporal resolution.

The use of 3D-FRAP enables the comparison of GJ permeability to miRNA under different conditions. To demonstrate this, we induced an siRNA-mediated knockdown of Cx43, leading to reduced protein expression (**Figure 3C**) and the inhibition of gap junctional communication. As a result, fluorescence recovery was reduced by more than 50%, indicating that the efficiency of miRNA transfer is strongly dependent upon the extent of gap junctional coupling between cells (**Figure 3B**, Cx43 knockdown). To confirm that the fluorescence recovery reflects the passage of the fluorescently labeled miRNA, rather than the detached Dy547-tag, we also acquired FRAP data for calcein dye (**Figure 3D**). Calcein has a molecular weight comparable to that of Dy547 and thus possess similar transfer dynamics. In contrast to the fluorescence recovery of Dy547-labeled miRNA, calcein demonstrated increased gap junctional exchange, indicating that the Dy547 tag is not detached from the miRNA molecule (**Figure 3D**).

Stable focus conditions are mandatory throughout a FRAP experiment, especially when long-term measurements are performed. Compared to 2D applications, 3D-FRAP can compensate for potential focus drift. As shown in **Figure 4**, even slight focus changes affect the proper detection of the fluorescence signal of miRNA when just a single 2D layer is used for the FRAP experiment (**Figure 4B**). In contrast, for 3D-FRAP, a whole z-stack of the target cell is recorded, and maximum projections are subjected to data analysis (**Figure 4A**). The impact of focus drift on a normalized fluorescence-intensity curves is depicted in **Figure 4C**. While fluorescence recovery steadily increases over time in 3D-FRAP, 2D-FRAP acquisition results in a decline of the fluorescence signal.

Beside the compensation of focus changes, 3D-FRAP also provides spatial data of the gap junctional exchange of miRNA. **Figure 5** shows a 3D surface rendering of a FRAP experiment. Compared to maximum projections, the acquisition of z-stacks can be used to create 3D reconstructions to investigate the localization and mobility of miRNA within cells (**Figure 5**). Co-labeling with organelles will allow for investigation into the involvement of other cellular components in miRNA transfer.

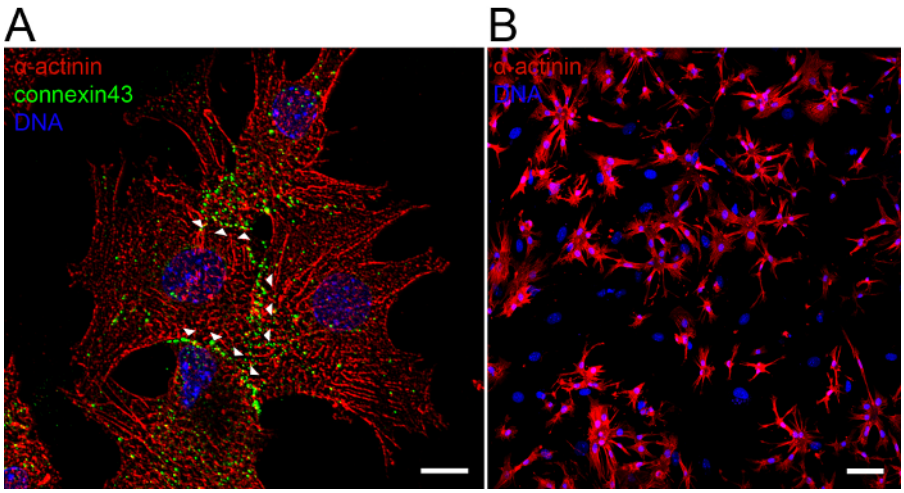

Figure 1: Representative Microscopic Images of Isolated Neonatal Cardiomyocytes. (**A**) Structured illumination microscopy shows the high expression of Cx43, which accumulates in large plaques at cell-cell borders (arrowheads). The pronounced formation of GJs with adjacent cells enables an extensive exchange of small molecules, including miRNA. Scale bar = 20 µm (**B**) Purity of isolated cardiomyocytes. Labeling of α-actinin demonstrates that cardiomyocytes represent the major cell type after isolation. Scale bar = 50 µm. Cells were stained with anti-Cx43 (green) and anti-α-actinin antibodies (red). Nuclei were visualized using DAPI (blue). A description of structured illumination microscopy and immunological labeling is provided in a previous publications[20]. Please click here to view a larger version of this figure.

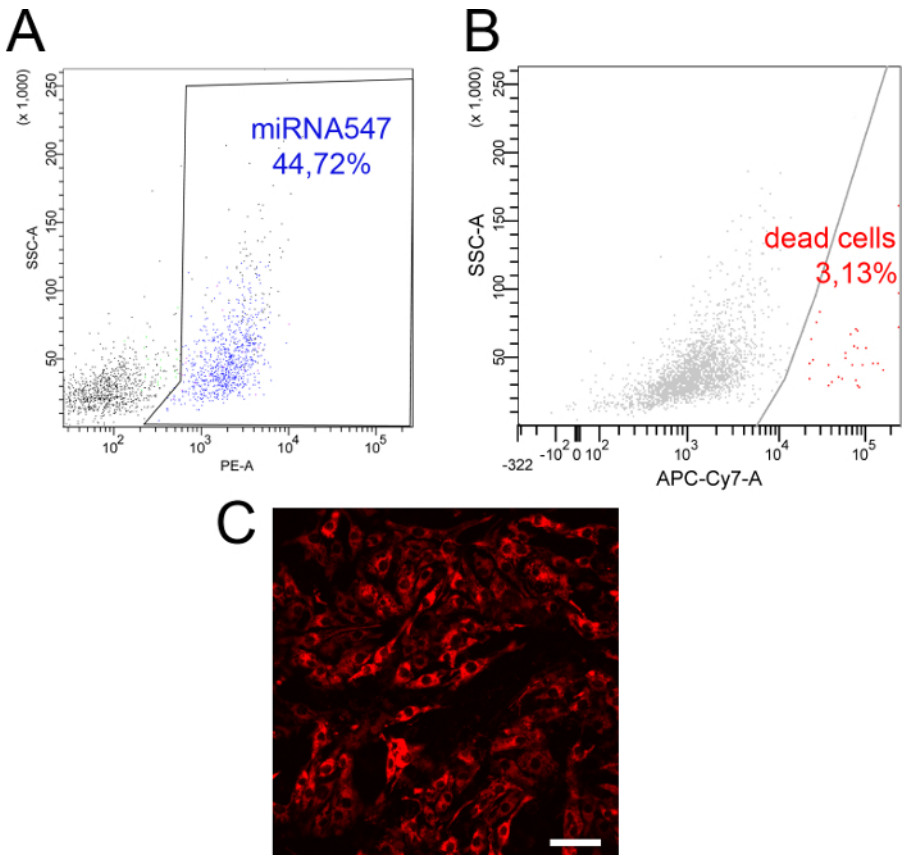

Figure 2: Transfection Efficiency, Viability, and Cell Density of Neonatal Cardiomyocyte culture. (**A**) Flow cytometry revealed that miR547 electroporation resulted in a transfection efficiency of ~45%. (**B**) Cell viability of cardiomyocytes used for FRAP. After isolation, electroporation, and reattachment, cardiomyocytes were subjected to live and dead cell staining and demonstrated high cell viability. (**C**) Microscopic image of mir547-transfected cardiomyocytes prepared for FRAP microscopy. A cell density of 80-90% ensures the pronounced formation of gap junctional cell-cell contacts. Scale bar = 50 µm. A method for the flow cytometric analysis of transfection efficiency and viability staining is mentioned in previous publications[20,21]. Please click here to view a larger version of this figure.

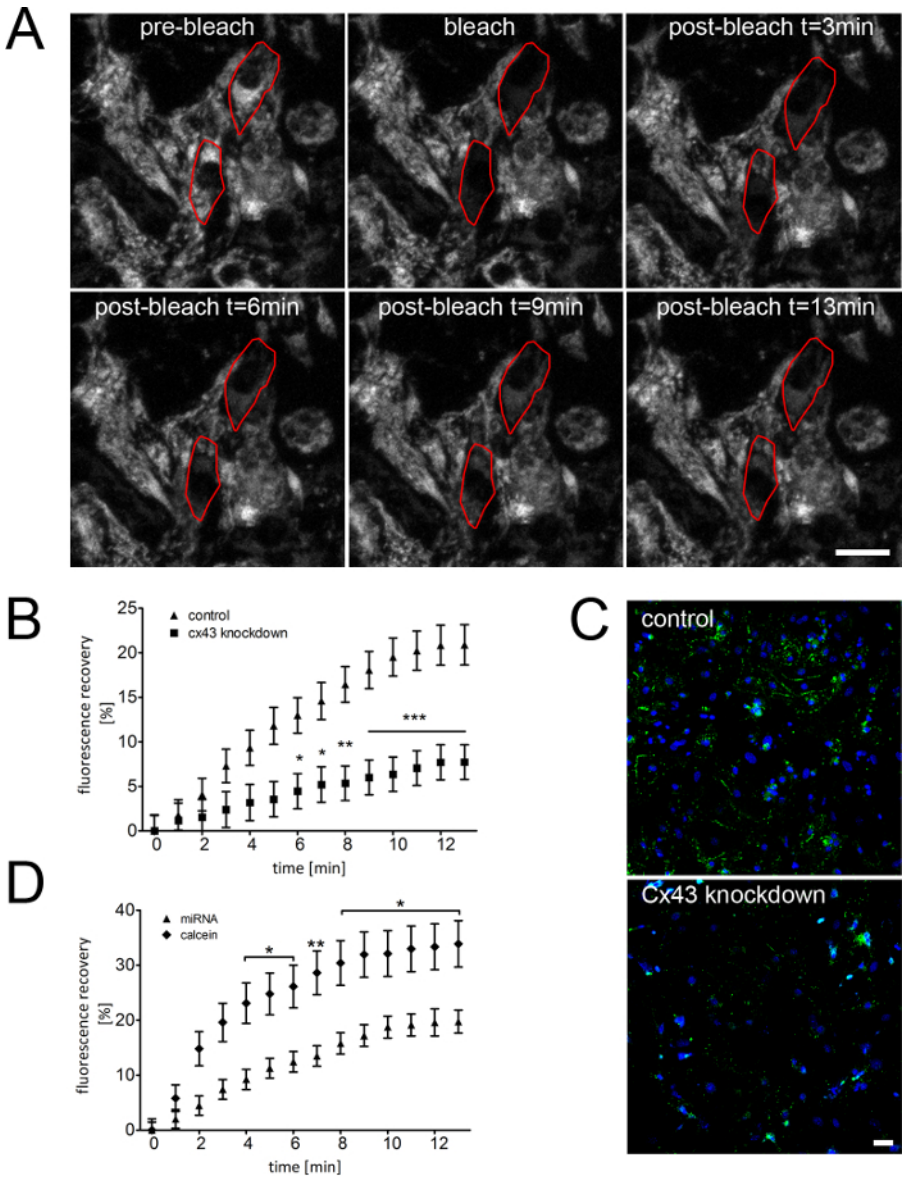

Figure 3: GJ-dependent Exchange of miRNA in Neonatal Cardiomyocytes. (**A**) Representative images of a FRAP experiment. After transfection with labeled miRNA, target cells within a cell cluster are photobleached by a strong laser pulse (pre-bleach versus bleach). Depending upon the extent of gap junctional coupling, the gap junctional influx of miRNA from adjacent cells results in increased fluorescence intensity in the bleached target cells (post-bleach t = 3, 6, 9, and 13 min). Scale bar = 20 µm (**B**) Quantitative analysis of acquired FRAP data shows a fluorescence recovery of 20% after 13 min. To confirm the involvement GJs in the intercellular transfer of miRNA, a cx43 knockdown was performed, leading to a strong decrease of fluorescence recovery (50%). (**C**) Immunostaining with anti-Cx43 antibody and subsequent confocal microscopy demonstrate the efficiency of the Cx43 knockdown at the protein level. Scale bar = 50 µm. (**D**) Comparison of the FRAP data of miR547 and calcein dye show the different transfer dynamics. The smaller molecular weight of calcein resulted in an increased fluorescence recovery compared to dy547-tagged miRNA molecules. FRAP curves summarize the data of n ≥56 cells, shown as the mean ± SEM. Statistical analysis was performed using two-way ANOVA followed by Bonferroni's post-hoc test (*P <0.05, **P <0.01, ***P <0.001). Please click here to view a larger version of this figure.

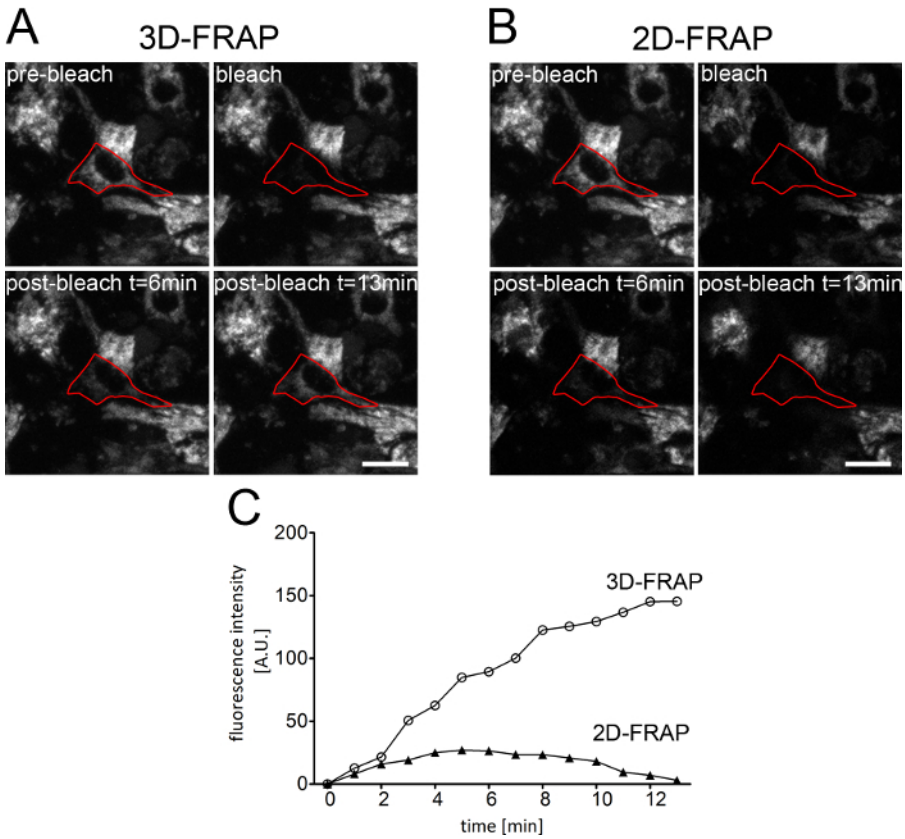

Figure 4: Compensation of Focus Drift using 3D-FRAP Microscopy. (**A** and **B**) Representative images of a photobleached cell (red line) demonstrate the impact of focus drift on the fluorescence intensity during 3D- and 2D-FRAP experiments. (**A**) In 3D-FRAP, z-stacks are recorded for each time-point, and maximum projections are used for data analysis, which corrects for focus drift. Scale bar = 20 µm. (**B**) In contrast, for 2D-FRAP, just a single 2D-layer is subjected to data analysis. Thus, the overall fluorescence intensity is profoundly reduced by changes in the focus. Scale bar = 20 µm. (**C**) Representative normalized fluorescence-intensity curves of 3D- and 2D-FRAP experiments indicate the strong effect of focus drift on fluorescence recovery and show the benefits of 3D acquisition when studying intercellular miRNA shuttling. Please click here to view a larger version of this figure.

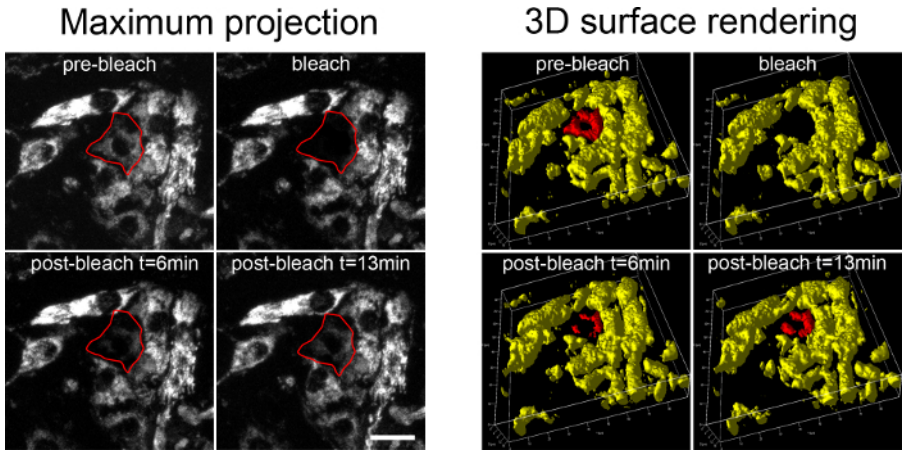

Figure 5: 3D Surface Rendering of a 3D-FRAP Experiment. (Left) Maximum projections of a FRAP measurement. The photobleached cell (red frame) demonstrates an increase in fluorescence intensity due to miRNA transfer from adjacent cells. (Right) Acquired z-stacks of the same photobleached cell (red) were subjected to 3D surface rendering to visualize the spatial distribution of the miRNA. Scale bar = 20 µm. Please click here to view a larger version of this figure.

Discussion

miRNAs are key players in cellular physiology and were shown to act as signaling molecules by using—among others—GJs as a pathway for intercellular exchange[11,12,22]. The current protocol presents an *in vitro* live-cell imaging technique to characterize this GJ-dependent shuttling using fluorescent miRNAs within cell clusters.

The protocol was developed on cardiomyocytes as a cell model system. However, this approach can be applied to several cell types if electroporation is a suitable method for miRNA transfection. In addition to cell-to-cell exchange, the presented technique is also suitable to investigate the intracellular mobility of miRNA molecules (*e.g.,* for the identification of possible transport mechanisms within the cell)[23,24].

The investigation of miRNA transfer by FRAP microscopy requires fluorescently tagged miRNA molecules (**Figure 2**). As the labeling of specific cellular miRNAs is not feasible, only exogenous, introduced labeled miRNA can be used for 3D-FRAP to analyze its intercellular mobility. In our experiments, cells were transfected with 250-nM miRNA. This concentration was much higher compared to physiological conditions, where the miRNA level ranges from 10 to 50,000 molecules per cell[27,28]. Such low concentrations cannot be used in FRAP experiments, as a certain level of fluorescent miRNA molecules is required to obtain a sufficient fluorescence signal and to ensure the proper discrimination between background fluorescence and fluorescently labeled miRNA. However, depending upon the confocal imaging system and the dye properties, the use of miRNA concentrations at low-nM range should be feasible for FRAP assays.

Different techniques are commonly applied to study intercellular miRNA transfer, including flow cytometry, PCR, and luciferase reporter assays[12,13]. These methods detect miRNA shuttling with low temporal resolution (*i.e.,* hours to days). In contrast, 3D-FRAP microscopy allows for the visualization and quantification of miRNA transfer and mobility in real time. In addition to gap junctional cell-cell contacts, the intercellular shuttling of miRNA is also mediated by other mechanisms, such as exosomes[18,29,30]. Only 3D-FRAP provides sufficiently high temporal resolution to discriminate between exosomal and gap junctional transfer. Thus, it allows for specific investigation into the direct effect of GJ permeability on miRNA signaling under different pathological or physiological conditions (**Figure 2**).

We recommend the use of 3D-FRAP, which is superior to conventional 2D-FRAP, as it provides more accurate data on GJ-dependent miRNA transfer. 3D-FRAP measurements include the entire cell volume, which is important when using large-bulk cell types. In addition, it can compensate focus changes or cell movements, which were shown to significantly impair fluorescence recovery in 2D-FRAP (**Figure 3**). Finally, the recording of z-stacks in 3D-FRAP experiments provides the possibility to obtain spatial information, which is not feasible when just a single 2D layer is used for the analysis of fluorescence intensities (**Figure 3B**).

Since fluorescence recovery is dependent upon the influx of miRNA from adjacent cells, the number of cells connected to the bleached cell is critical and must be similar across different measurements to obtain reliable data. Therefore, a high cell density is required to ensure the formation of cellular clusters most suitable for FRAP analysis. Furthermore, preliminary experiments must be performed to select mild bleaching conditions (*i.e.,* laser power, bleaching time, and scan settings) to avoid phototoxic effects caused by a high laser intensity[25,26]. This will also help to reduce the photobleaching that occurs during the acquisition process.

Despite the limitations, our data show that 3D-FRAP is a powerful tool to evaluate the role of miRNAs as signaling molecules within a cellular network. The impact of connexin composition on miRNA shuttling or the selective permeability of GJs for specific miRNAs can be addressed with the direct quantification of transport efficiency. 3D-FRAP can provide important information to improve the development of new therapies featuring miRNA and siRNA, such as by defining proper conditions that facilitate the distribution of small RNAs *via* the GJ network[31,32].

Disclosures

The authors declare no conflict of interest.

Acknowledgements

This work was supported by the Federal Ministry of Education and Research Germany (FKZ 0312138A and FKZ 316159), the State Mecklenburg-Western Pomerania with EU Structural Funds (ESF/IVWM-B34-0030/10 and ESF/IVBM-B35-0010/12), the DFG (DA1296-1), and the German Heart Foundation (F/01/12). In addition, R.D. is supported by the FORUN Program of Rostock University Medical Centre (889001), the DAMP Foundation, and the BMBF (VIP+ 00240).

References

1. Carthew, R. W., Sontheimer, E. J. Origins and Mechanisms of miRNAs and siRNAs. *Cell.* **136** (4), 642-655 (2009).
2. Fire, A., Xu, S., Montgomery, M. K., Kostas, S. A., Driver, S. E., Mello, C. C. Potent and specific genetic interference by double-stranded RNA in Caenorhabditis elegans. *Nature.* **391** (6669), 806-811 (1998).
3. Grimm, D. Small silencing RNAs: state-of-the-art. *Adv Drug Deliv Rev.* **61** (9), 672-703 (2009).
4. Raghunathan, S., Patel, B. M. Therapeutic implications of small interfering RNA in cardiovascular diseases. *Fundam Clin Pharmacol.* **27** (1), 1-20 (2013).
5. Sluijter, J. P. G. MicroRNAs in Cardiovascular Regenerative Medicine: Directing Tissue Repair and Cellular Differentiation. *ISRN Vasc Med.* **2013**, 1-16 (2013).
6. Li, M., Zhang, J. Circulating MicroRNAs: Potential and Emerging Biomarkers for Diagnosis of Cardiovascular and Cerebrovascular Diseases. *Biomed Res Int.* **2015**, 1-9 (2015).
7. Romaine, S. P. R., Tomaszewski, M., Condorelli, G., Samani, N. J. MicroRNAs in cardiovascular disease: an introduction for clinicians. *Heart.* **101** (12), 921-8 (2015).
8. Maes, M., Crespo Yanguas, S., Willebrords, J., Cogliati, B., Vinken, M. Connexin and pannexin signaling in gastrointestinal and liver disease. *Transl Res.* **166** (4), 332-343 (2015).
9. Michela, P., Velia, V., Aldo, P., Ada, P. Role of connexin 43 in cardiovascular diseases. *Eur. J. Pharmacol.* **768**, 71-76 (2015).
10. Naus, C. C., Laird, D. W. Implications and challenges of connexin connections to cancer. *Nat Rev Cancer.* **10** (6), 435-441 (2010).
11. Hong, X., Sin, W. C., Harris, A. L., Naus, C. C. Gap junctions modulate glioma invasion by direct transfer of microRNA. *Oncotarget.* **6** (17), 15566-15577 at <www.impactjournals.com/oncotarget> (2015).

12. Lee, H. K. H. *et al.* Mesenchymal stem cells deliver synthetic microRNA mimics to glioma cells and glioma stem cells and inhibit their cell migration and self-renewal. *Oncotarget.* **4** (2), 346-361, (2013).
13. Katakowski, M., Buller, B., Wang, X., Rogers, T., Chopp, M. Functional microRNA is transferred between glioma cells. *Cancer Res.* **70** (21), 8259-8263 (2010).
14. Zong, L., Zhu, Y., Liang, R., Zhao, H.-B. Gap junction mediated miRNA intercellular transfer and gene regulation: A novel mechanism for intercellular genetic communication. *Sci Rep.* **6** (January), 19884 (2016).
15. Yum, S. W., Zhang, J., Scherer, S. S. Dominant connexin26 mutants associated with human hearing loss have trans-dominant effects on connexin30. *Neurobiol Dis.* **38** (2), 226-236 (2010).
16. Kuzma-Kuzniarska, M., Yapp, C., Pearson-Jones, T. W., Jones, A. K., Hulley, P. A. Functional assessment of gap junctions in monolayer and three-dimensional cultures of human tendon cells using fluorescence recovery after photobleaching. *J Biomed Opt.* **19** (1), 15001 (2013).
17. Lemcke, H., Nittel, M.-L., Weiss, D. G., Kuznetsov, S. A. Neuronal differentiation requires a biphasic modulation of gap junctional intercellular communication caused by dynamic changes of connexin43 expression. *Eur J Neurosci.* **38** (2), 2218-2228 (2013).
18. Lemcke, H., Steinhoff, G., David, R. Gap junctional shuttling of miRNA - A novel pathway of intercellular gene regulation and its prospects in clinical application. *Cell Signal.* **27** (12), 2506-2514 (2015).
19. Lemcke, H., Kuznetsov, S. A. Involvement of connexin43 in the EGF/EGFR signalling during self-renewal and differentiation of neural progenitor cells. *Cell Signal.* **25** (12), 2676-2684 (2013).
20. Lemcke, H., Peukert, J., Voronina, N., Skorska, A., Steinhoff, G., David, R. Applying 3D-FRAP microscopy to analyse gap junction-dependent shuttling of small antisense RNAs between cardiomyocytes. *J. Mol. Cell. Cardiol.* **98**, 117-127 (2016).
21. Laupheimer, M. *et al.* Selective Migration of Subpopulations of Bone Marrow Cells along an SDF-1 α and ATP Gradient. *Bone Marrow Res.* **2014**, 1-10 (2014).
22. Zhang, S., Wang, Q., Liu, L., Hong, X., Zhang, Y., Tao, L. Gap junctions enhance the antiproliferative effect of microRNA-124-3p in glioblastoma cells. *J Cell Physiol Physiol.* **230** (10), 2476-2488 (2015).
23. Vasilescu, C., Tanase, M., Dragomir, M., Calin, G. A. From mobility to crosstalk. A model of intracellular miRNAs motion may explain the RNAs interaction mechanism on the basis of target subcellular localization. *Math Biosci.* **280**, 50-61 (2016).
24. Pitchiaya, S., Androsavich, J. R., Walter, N. G. Intracellular single molecule microscopy reveals two kinetically distinct pathways for microRNA assembly. *EMBO Rep.* **13** (8), 709-15 (2012).
25. Heinze, K. G., Costantino, S., De Koninck, P., Wiseman, P. W. Beyond photobleaching, laser illumination unbinds fluorescent proteins. *J Phys Chem B.* **113** (15), 5225-5233 (2009).
26. Jou, M. J., Jou, S. Bin, Guo, M. J., Wu, H. Y., Peng, T. I. Mitochondrial reactive oxygen species generation and calcium increase induced by visible light in astrocytes. *Ann N Y Acad Sci.* **1011**, 45-56 (2004).
27. Dong, H., Lei, J., Ding, L., Wen, Y., Ju, H., Zhang, X. MicroRNA: Function, detection, and bioanalysis. *Chem Rev.* **113** (8), 6207-6233 (2013).
28. Liang, Y., Ridzon, D., Wong, L., Chen, C. Characterization of microRNA expression profiles in normal human tissues. *BMC Genomics.* **8** (1), 166 (2007).
29. Mittelbrunn, M. *et al.* Unidirectional transfer of microRNA-loaded exosomes from T cells to antigen-presenting cells. *Nat Commun.* **2**, 282 (2011).
30. Squadrito, M. L. *et al.* Endogenous RNAs Modulate MicroRNA Sorting to Exosomes and Transfer to Acceptor Cells. *Cell Rep.* **8**, 1432-1446 (2014).
31. Zhang, B., Farwell, M. a microRNAs: a new emerging class of players for disease diagnostics and gene therapy. *J Cell Mol Med.* **12** (1), 3-21 (2008).
32. Chen, Y., Gao, D.-Y., Huang, L. In vivo delivery of miRNAs for cancer therapy: Challenges and strategies. *Adv Drug Deliv Rev.* **81C**, 128-141 (2015).

